Research Article

Chenglong Zhao, Yan Qin*, Xiaotian Wang, and Han Xiao

Coefficient of thermal expansion and mechanical properties of modified fiber-reinforced boron phenolic composites

https://doi.org/10.1515/epoly-2022-0036 received December 14, 2021; accepted March 18, 2022

Abstract: Boron phenolic resin is widely used in the aerospace field because of its excellent thermal properties. In this article, nitrile rubber powder was added to phenolic resin to modify fiber-reinforced phenolic resin composites. The results showed that the tensile strength continued to decrease; the elongation ratio increased from 20.01% to 32.04%; and flexural strength and flexural modulus reached the highest values of 188 and 9,401 MPa, respectively. Thermal analysis showed that rubber had little effect on the heat resistance at low temperatures, especially below 350°C. Furthermore, the coefficient of thermal expansion of the composites increased from 8.9×10^{-6} to 1.5×10^{-5} K⁻¹, increasing by nearly 70%. The electron microscopy images showed a tortuous fracture path in modified composites, which indicated that rubber powder-modified phenolic composites had a ductile fracture.

Keywords: boron phenolic resin, composites, thermal performance, nitrile rubber, microstructure

1 Introduction

With the development of aerospace technology, thermal protection systems have been paid much attention by researchers. Fiber-reinforced composites have been applied in the aerospace field as ablation and heat protection materials (1). Researchers focus much on ablation resis-

tance and process performance of polymer composites but paid less attention to the interfacial thermalmatching properties of composites and metal materials. The coefficient of thermal expansion (CTE) in a typical aluminum alloy is $20-300 \times 10^{-6} \,\mathrm{K}^{-1}$, which is much higher than $5-8 \times 10^{-6} \,\mathrm{K}^{-1}$ of fiber-reinforced composites. This article aims to improve the CTE of resin composites to the level of the CTE of alloys. The temperature difference between the inner and the outer layer of a heat protection system, as well as metal components, causes linear expansion and pyrolysis expansion. It is prone to thermal stress and deteriorates the properties and structure of interface material (2-4). When the interfacial layers of metal structures and composites are peeled off from the interior, the external thermal protection material would lose its protective function.

The interface material is a transition component. It faces lower temperatures and does not require excellent thermal stability. Carbon fiber is not considerable because of its low thermal expansion coefficient (even no expansion). Boron phenolic resin (BPF) has high thermal properties and has a good development prospect in the aerospace field (5,6). However, BPF is poor in toughness, and its composites and metal components have significantly different thermal expansion characteristics when heated (7,8). Composites bonded to the metal structure lose effectiveness, and the overall structure is easy to fail under high-speed airflow scouring, threatening flight security (9,10). It is necessary to modify the phenolic resin (PF) and study its thermal-matching characteristics (10–13).

Physical improvement is the main method for modifying PF aiming for more polymer chains between the cured phenolic molecules (14,15), accompanied by a small number of chemical reactions. It has a wide range of applications because of its simplicity and low cost. Yan et al. (16) added 60 wt% graphite and 10 wt% carbon fiber to PF to improve the bending strength and modulus of the composite material. Liu et al. (17) noticed that when adding 2.5 wt% styrene-butadiene rubber nanoparticles, the notched impact strength of nanocomposites reached

^{*} Corresponding author: Yan Qin, School of Materials Science and Engineering, Wuhan University of Technology, Wuhan, China, e-mail: qinyan@whut.edu.cn

Chenglong Zhao, Xiaotian Wang, Han Xiao: School of Materials Science and Engineering, Wuhan University of Technology, Wuhan, China

the maximum value and was increased by 52%. Kazemi et al. (18) found that the hybrid titanium composite laminates with ultra-high-molecular-weight polyethylene fabrics on their composite sides performed better in low-velocity impact compared to composites with carbon fibers. The chemical modification changes the molecular structure to solve the defect of the resin. They have relatively high requirements for experiments, as well as a better guarantee of heat resistance and mechanical properties. Song et al. (19) showed better damping performance of composites at higher temperatures by introducing hindered amines into nitrile-butadiene rubber (NBR)/PF. Sekhar and Varghese (20) studied PF and modified graphite additives and obtained relaxation time information regarding regression parameters. Wang et al. (21) synthesized polyhedral oligomeric silsesquioxane-modified PF and proved that the modified PF had higher anti-oxidation properties than pure resin.

We select powdered form of BPF and NBR for material preparation. Compared to epoxy systems and other resins (22), BPF achieves a stable property transition of internal and external materials and eliminates excess interface with thermal-protected phenolic materials. NBR is a kind of effective physical agent. The compatibility of NBR with PF is better than that with general rubber (23). Furthermore, active functional groups of NBR may also react with PF, making the modification effect more significant. In this case, physical improvement is more convenient and easily implemented compared with chemical modification (24). Compared with rubber/resin research, we use powder NBR and avoid the "reaction-induced phase separation" effect on results. CTE is used to characterize the thermal-matching characteristics to discuss the suitability of materials from thermal properties. Fiber additions are more suitable for practical use.

Therefore, in this article, NBR-modified fiber-reinforced boron phenolic composites (NBR/BPF) were prepared. The main aim was to improve the CTE of phenolic composites while ensuring mechanical properties. We also strive to protect the interface of resin composites and metal structures under heating, aiming to maximize the CTE of resin composites to the level of alloys. The effects of NBR on curing, mechanical properties, thermal stability, microstructure, and thermal matching of composites were discussed. Analyses and results were confirmed by Fourier transform infrared (FTIR) spectrometry, mechanical tests, thermal tests, dynamic mechanical analysis (DMA), and scanning electron microscopy (SEM).

2 Experimental section

2.1 Materials and instruments

BPF produced by Shaanxi Taihang Impede Fire Polymer Co. Ltd. (China) was used as the matrix material. Orthogonal glass fiber produced by Shaanxi Huate New Material Co. Ltd. (China) was used as the reinforcement material, with 97% SiO_2 and $248.3\,\mathrm{g\cdot cm^{-3}}$ areal density. Anhydrous ethanol produced by Sinopharm Chemical Reagent Co. Ltd. (China) was used as a solvent. NBR powder produced by Guangzhou Qizhou Plasticization Company (China) was selected as the modified materials, with a particle size of $60-70\,\mu\mathrm{m}$ (distribution consistency of 80%). More details are given in Table 1.

The equipment used in the experimental process are a pulverizer (YK160, Jiangyin Shenwei Machinery Co. Ltd., China), an electronic balance (JA3003N, Scientific Instrument Co. Ltd., China), a flat vulcanizer (QLB-3 \times 350 \times 2–0.25 MN, Shanghai Rubber Machinery Factory, China), a vacuum drying oven (DZ-2BCII, Tianjin Teller Instrument Co. Ltd., China), and a stirrer (JB50-D, Shanghai Specimen Model Factory, China).

2.2 Preparation of composites

For pretreatment, the glass fiber was dried at 60°C for 5 h in a vacuum drying oven. The block resin to be pulverized was placed in a pulverizer. The powdered BPF was dissolved in anhydrous ethanol, leaving it still for 24 h. NBR powder was added in the resin solution. The mixture was placed on the stirrer and stirred for 30 min until the powder dispersed well. Glass fiber was impregnated with the homogeneous mixture. The formulations of NBR/BPF composites based on different powder contents, as long as numbering composite samples (from A-0 to A-5), are given in Table 2.

Table 1: Composites of NBR powder

Component	Volatile	Gel content	Acrylonitrile	Dissolved matter
Mass fraction (wt%)	0.5	91	31.7	0.6

Table 2: The formulation of NBR/BPF composites

Samples	Mass ratio (wt%)			
	Glass fiber	BPF	NBR powder	
A -0	50	50	0	
A-1	50	45.4	4.6	
A-2	50	41.7	8.3	
A-3	50	38.5	11.5	
A-4	50	35.7	14.3	
A-5	50	33.3	16.7	

Prepregs were all laid up in the direction of fiber stretch (0°) when laminated. The prepregs were cropped into 16 pieces (120 mm \times 90 mm) for molding, and the NBR/BPF composites were obtained after curing in a flat vulcanizer. The process of composite preparation is shown in Figure 1.

The curing temperature system is 120° C for $0.5 \, h + 150^{\circ}$ C for $0.5 \, h + 180^{\circ}$ C for $3 \, h$. The curing pressure system is $0 \, MPa$ for $0.5 \, h + 10 \, MPa$ for $3.5 \, h$. More details about the curing process are shown in Figure 2.

3 Material testing and performance characterization

3.1 Infrared analysis (FTIR)

Molecular structures of resin and NBR powder were analyzed using an intelligent FTIR spectrometer (Thermo

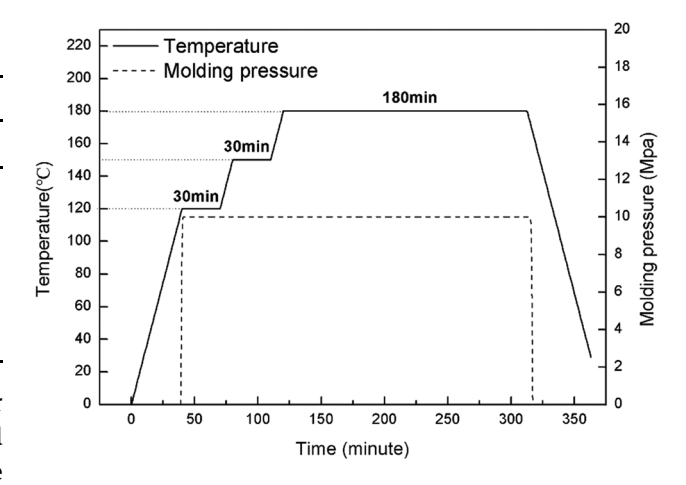


Figure 2: Cure profile for the fabrication of composites.

Nicolet Nexus, USA). The samples were ground into powder for examination.

3.2 Mechanical test

The tensile strength and elongation ratio were determined using a mechanical testing machine at a loading rate of 2 mm·min⁻¹ (CTM001, Instron, England) according to the GB/T 16421-1996 standard. Samples were processed into a dumbbell shape, 75 mm long and 5 mm at the narrowest part of the neck. The sample was tested until it broke, and the result was obtained. Five samples per formulation were arranged to measure and calculate the average tensile strength, elongation ratio, and their errors.

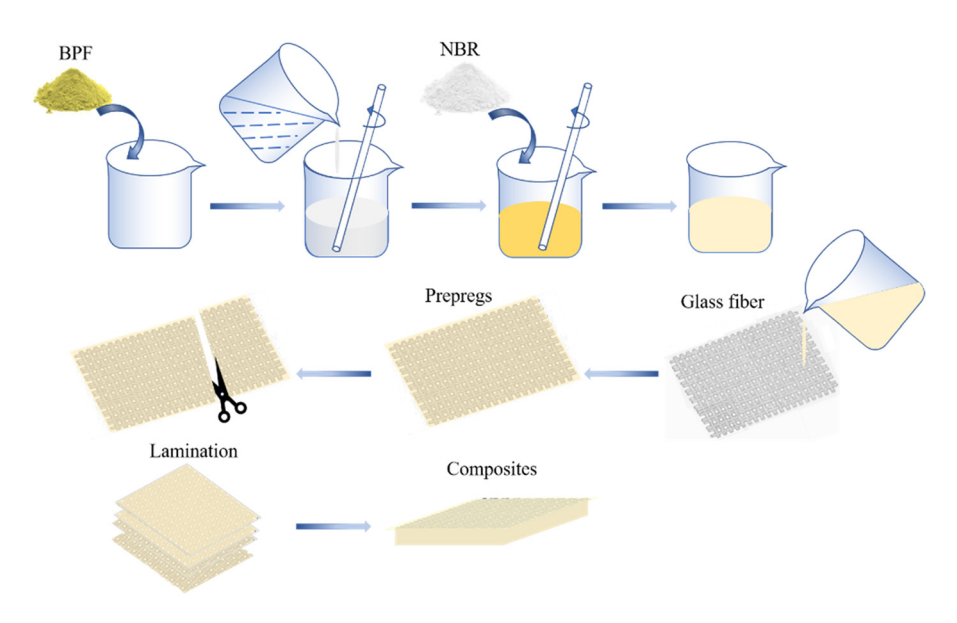


Figure 1: Process of composite preparation.

The tensile strength was calculated according to the following equation:

$$\alpha = \frac{P}{bh} \tag{1}$$

where α is the tensile strength (MPa), P is the breaking load (N), and b and h are width and thickness, respectively (mm).

The elongation ratio was calculated according to the following equation:

$$e = \frac{\Delta l}{l} \times 100\% \tag{2}$$

where e is the elongation ratio (%), Δl is the elongation (mm), and l is the original span (25 mm).

The flexural strength and flexural modulus of samples were determined by a mechanical testing machine with a loading rate of $2\,\mathrm{mm\cdot min^{-1}}$ (CTM001; Instron, England) according to the GB/T 1449-2005 standard. The effective size of the samples was 80 mm \times 15 mm \times 4 mm. The sample was tested by the "three-point bending test" until it broke and the result was obtained. Five samples per formulation were arranged to measure and calculate the average flexural strength, flexural modulus, and their errors.

The flexural strength was calculated according to the following equation:

$$\sigma = \frac{3Pl}{2hh^2} \tag{3}$$

where σ is the flexural strength (MPa), P is the breaking load (N), l is the span of the sample (64 mm), and b and h are the width and the thickness of the sample, respectively (mm).

The flexural modulus was calculated according to the following equation:

$$E = \frac{Sl^3}{4hh^3} \tag{4}$$

where E is the flexural modulus (MPa), S = F/d, d is the displacement corresponding to F in the load–displacement curve, l is the span of the sample (64 mm), and b and b are the width and the thickness, respectively (mm).

3.3 Thermal test

Thermal stability was observed with a high-temperature TG-DSC thermal analyzer (STA-449F3, NETZSCH, Germany). The heating rate was $10^{\circ}\text{C}\cdot\text{min}^{-1}$, and the test was performed in the air atmosphere. CTE was determined with a thermal expansion instrument (DIL402SE, NETZSCH,

Germany). The heating rate was 5°C·min⁻¹, and the temperature range was 20–300°C in the nitrogen atmosphere.

3.4 DMA

DMA was carried out in nitrogen using a dynamic thermomechanical analyzer (DMA/SDTA 861e, METTLER TOLEDO, Switzerland), at a heating rate of $5^{\circ}\text{C·min}^{-1}$ from -70°C to 400°C and a frequency of 1 Hz. The size of the samples was $60 \text{ mm} \times 10 \text{ mm} \times 4 \text{ mm}$.

3.5 Performance characterizations

The cross sections and interfaces of the original sample and NBR/BPF composites were observed by a field-emission scanning electron microscope (Ultra Plus, Zeiss, Germany). The sample was gold-plated before observation.

4 Results and discussion

4.1 FTIR spectrum analysis

Figure 3 shows the FTIR spectra of the composites with different powder contents. The FTIR peaks marked at 3,427 and 3,226 cm⁻¹ are the characteristic absorption peaks of the O–H bond on BPF. The peak marked at

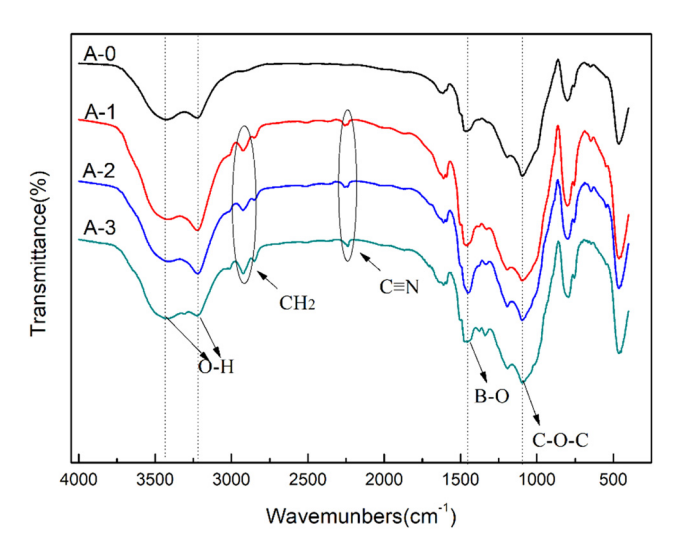


Figure 3: FTIR spectra of the composites.

1,453 cm⁻¹ is the characteristic peak of the B-O bond on resin The peak marked at 1,096 cm⁻¹ is the C-O-C symmetric stretching vibration absorption peak on the benzene ring. It can be clearly seen from Figure 3 that there are two more obvious absorption peaks in the spectrum of the composites with NBR: 2,258 cm⁻¹ corresponds to the C=N characteristic absorption peak of NBR and 2,925 cm⁻¹ corresponds to the CH₂ characteristic absorption peak of asymmetric stretching vibration in NBR. The curves of A-1, A-2, and A-3 do not prove chemical reaction occurrence, because only the shift and intensity changes of the peaks are favorable evidence for the reaction. The FTIR result shows that there is no obvious peak shift and intensity change. The FTIR spectrum could not prove that a chemical reaction occurred but preserves the possibility of a grafting reaction between NBR and PF. The three possible reactions that occur between PF and NBR are shown in Figure 4.

4.2 Mechanical properties

Mechanical tests are carried out in the direction of fiber stretch (0°). Figure 5 shows the effect of NBR on the tensile property and elongation ratio of composites. Figure 6 shows the effect of NBR on the flexural properties. As shown in Figure 5, powder leads to a decrease in the tensile strength of the composites and an increase in the elongation ratio. The tensile strength of the A-0

Figure 4: Reaction mechanism of BPF and NBR.

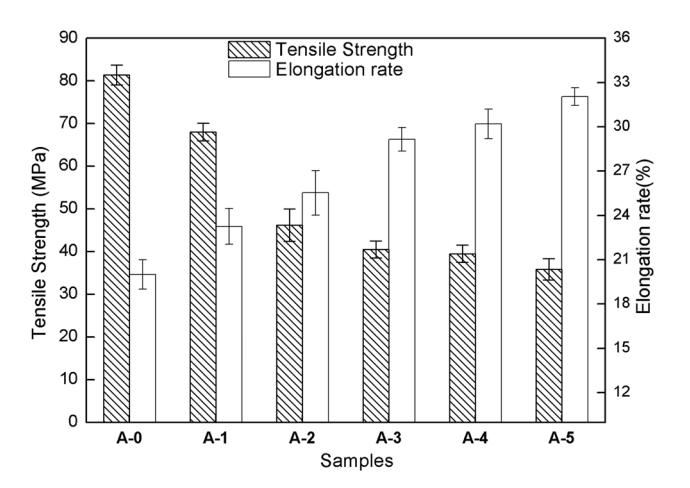


Figure 5: Tensile strength and elongation ratio of composites.

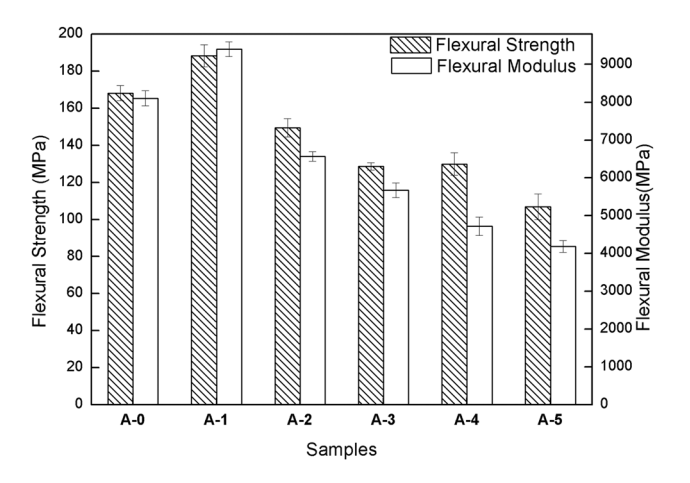


Figure 6: Flexural strength and flexural modulus of composites.

sample reaches 81.4 MPa. The tensile strength of the A-5 sample is 55% less than that of A-0. The elongation ratio increases from 20.01% for A-0 to 32.04% for A-5. It is suggested that the NBR powder can act as stress concentrators around the composites and cause yielding. It is capable of inducing an energy dissipation mechanism in the composites during the tensile deformation. Accordingly, the polymer absorbs a high amount of energy and avoids a highly localized strain process. When composites are stressed, they interact with rigid molecules such as PF, increasing the elongation ratio.

As can be seen from Figure 6, the NBR powder content has an effect on the flexural property. It is interesting to observe that the strength of A-1 is the highest. The flexural strength of the composites without powder reaches 169 MPa, but that of A-1 reaches 188 MPa. Its strength is greater than 149 MPa of other fiber-reinforced phenolic composites (25,26). On the one hand, rubber destroys the

interfacial bond between fibers and resin. The rubber is not only hard to bond with the fiber, but it also occupies space for the resin, preventing the benign bond between the resin and the fiber. Although powder contains reactive groups, NBR itself has been vulcanized, leading to a poor toughening effect. On the other hand, NBR powder can fill the holes caused by the release of small molecules during resin curing, and filled composites can support higher forces. The reinforcing effect of rubber particles is temporarily more obvious, resulting in the flexural strength of A-1 to be the largest. The trends of the strength and modulus are the same. The modulus of composites reaches a maximum of about 9,401 MPa in A-1, and the modulus decreases to only 4,186 MPa in A-5. When the powder content increases, its dispersibility becomes worse and agglomeration occurs. The resin-fiber interface is occupied by rubber, and it becomes worse, resulting in a decrease in the strength and modulus of the composites.

4.3 Thermal test

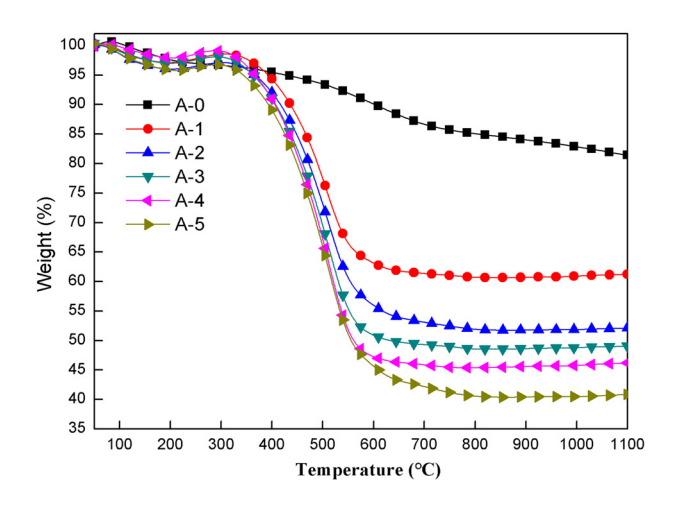
Figure 7 shows the thermogravimetry (TG) and derivative thermogravimetry (DTG) curves of composites. The TG chart can be divided into two stages. The first stage is from 50°C to 300°C. In this stage, the curve is in the volatilization period with smooth change. The decomposition rate near 100°C was attributed mainly to the evaporation of water and other molecules in samples. However, the A-1 to A-5 samples show a slight increase in mass after a slight weight loss. We speculate that the pyrolysis of rubber components activates the oxygen-

absorbing behavior of BPR. The second stage is from 300°C to 600°C. In this stage, the curves decrease sharply, and the weight loss is obvious due to resin cracking and rubber decomposition. For the A-0 sample, cracking PF produces CO and CO₂. When the temperature increases, the main chain of BPF cracks, the structure rearranges, and then BO, B2O3, and other products are released. For A-1 to A-5 samples, rubber decomposes into small molecules and escapes. Table 3 shows their thermal decomposition parameters. We find that NBR powder reduces the heat resistance of composites significantly. With an increase in powder content, the initial decomposition temperature of the composites decreases from 427.6°C to 343.5°C. We analyze T_5 and T_{30} in Table 3 and find that $T_{\text{heat-resistance index}}$ (27-29) of the composites shows a continuous downward trend. With an increase in the rubber component, $T_{\text{heat-resistance index}}$ of the rubbercontaining component decreased from 232.6°C to 210.4°C. The residuals of composites at 600°C continue to decrease (30).

As can be seen from Figure 7, TG curves of rubber-containing composites decrease sharply after 500°C, but the heat resistance is seldom affected at low temperatures. The thermal weight loss at 400°C is ideal, and the residual weight at 300°C is, on average, 1.1% higher than those reported in other papers (31). NBR powder reduces heat resistance, but it has little effect on heat resistance at low temperatures (below 350°C). Because the materials are used between the metal and the outer protective structure, it does not face high-temperature erosion. Rubber has little effect on the heat resistance of the actual demand of the material.

CTE is carried out in the direction of fiber stretch (0°). Figure 8 shows the CTE curves of composites, and Table 4

0.0



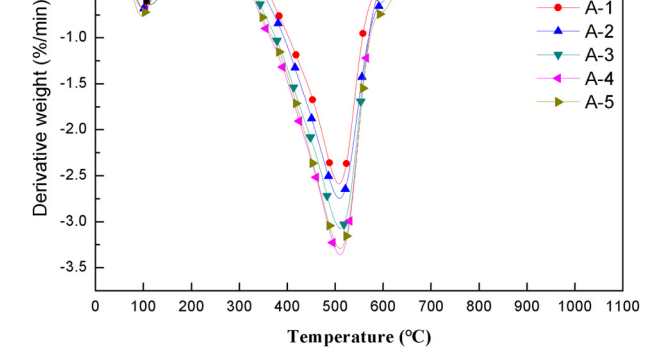


Figure 7: TG and DTG curves of composites.

Table 3: Thermal decomposition parameters of NBR/BPF composites

Samples	<i>T</i> ₅ (°C)	<i>T</i> ₃₀ (°C)	Theat-resistance index (°C)	T _{max1} (°C)	T _{max2} (°C)	Residue (600°C, %)
A-0	427.6	_	_	115.6	117.4	90.1
A-1	392.5	529.5	232.6	99	507	63.1
A-2	366.2	510.7	221.9	100.2	508.7	56.0
A-3	362.5	498	217.5	98.5	510.5	50.9
A-4	366.5	491	216.2	110	509.5	47.3
A-5	343.5	486.5	210.4	95.5	510.5	45.7

 T_5 and T_{30} are the corresponding decomposition temperatures of 5% and 30% weight loss, respectively.

The heat-resistance index was calculated according to the following equation: $T_{\text{heat-resistance index}} = 0.49 \times [T_5 + 0.6 \times (T_{30} - T_5)]$, where $T_{\text{max}1}$ and $T_{\text{max}2}$ are the corresponding decomposition temperatures corresponding to the maximum thermal decomposition rate for the first and second occurrences.

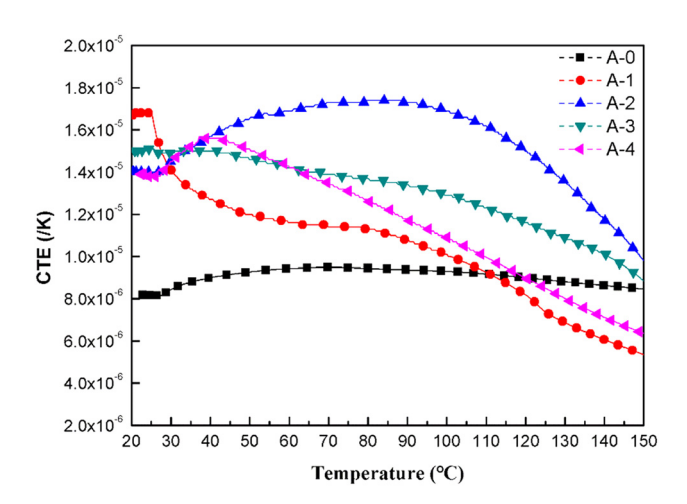


Figure 8: CTE curve of composites.

Table 4: Average CTE of composites

Samples	A-0	A-1	A-2	A-3	A-4
CTE (10 ⁻⁶ K ⁻¹)	8.9	10.8	15.0	13.1	11.5

shows the average CTE. NBR powder increases the CTE of composites. For the A-0 sample, the CTE is about $8\times 10^{-6}\,\mathrm{K^{-1}}-9\times 10^{-6}\,\mathrm{K^{-1}}$. The CTE of the A-2 sample reaches the maximum value of $1.5\times 10^{-5}\,\mathrm{K^{-1}}$. As the NBR powder further increases, the CTE of composites does not continue to increase but slightly decreases. Rubber is elastic at room temperature. Because of the low glass-transition temperature, it tends to produce large deformations when heated or stressed. The volume expands and the CTE increases significantly without destruction when heated. For A-1 and A-2, the powder disperses evenly and combines well with the resin (32). When the

rubber is more than 20 phr, the NBR powder is prone to agglomeration. Agglomerated powders can lead to poor rubber-resin and resin-fiber interfaces. The deteriorated interface leads to a smaller expansion contribution of the powder to composite, resulting in a decrease in CTE.

We find that the CTE of the rubber-modified materials decreases after 110°C. The growth rate of rubber diameter is not synchronized with the volume growth rate, leading to CTE decreases. In addition, the evaporation of molecules results in porosity increase, making rubber expansion unable to effectively transfer to the resin matrix. These two main factors lead to the lower CTE of rubbermodified materials above 110°C.

4.4 DMA

DMA is carried out in the direction of fiber stretch (0°). Loss factor versus temperature curves of composites and pure BPF are presented in Figure 9. All four curves have a typically broad peak at about 250°C corresponding to T_{σ} of resin. Due to voids and bubbles in the cured resin, the curve of pure BPF shows broad and heterogeneous peaks on DMA. The curve of A-0 has a peak at 270°C, and the peak of PF tends to move toward low temperatures with powder addition. There are two peaks in the plots of NBR/BPF (A-1 and A-2). $T_{\rm g}$ of NBR in the literature is -12°C (33). The peaks at near 10°C, corresponding to the $T_{\rm g}$ of NBR in composites or the secondary transition of PF segments, reveal that the $T_{\rm g}$ of NBR in composites is higher than that of pure NBR or that the addition of NBR leads to a more obvious secondary transition of PF segments (17). Another set of peaks appeared at around 250°C. DMA reflects the phase situation of the blend system from the side. Chemically modified PFs tend to show only a single peak in the DMA test, while physically

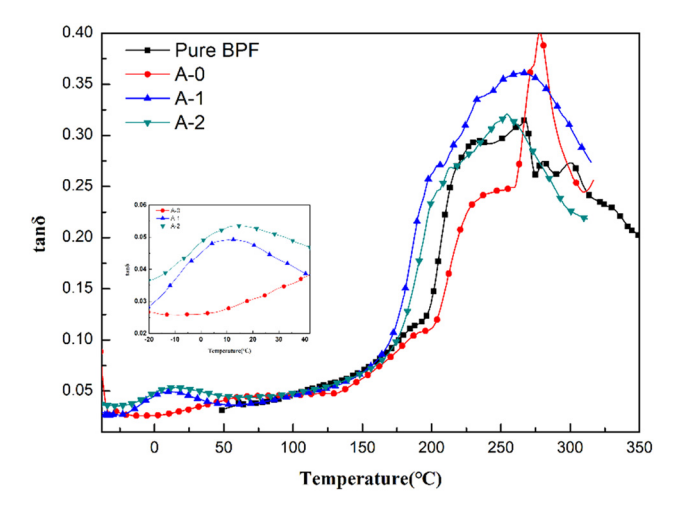


Figure 9: $\tan \delta$ of the composites with temperature.

blend-modified PFs show bimodal or multimodal peaks. Physical modification does not change the molecular structure of PFs. During curing, the rubber component cannot enter the cross-linked network of PF, resulting in phase separation in the cured product, and a peak appears in the low-temperature area in modified composites.

4.5 Morphology analysis

The morphology of tensile fracture is shown by SEM analysis in Figure 10. Fiber, rubber, and holes are marked in the figure. The tensile section of A-O can be seen clearly

in Figure 10a. The fracture is flat and almost no fiber is pulled out, which is a typical brittle fracture at the lower magnification. Resin is evenly distributed between the fibers, and the fracture of fibers is almost at the same level at the higher magnification (34). From Figure 10b, the fiber is wrapped with resin and the fracture is uneven. Fibers have no neat ports in cross section compared with those shown in Figure 10a. The SEM image shows a tortuous fracture path. Compared with Figure 10a, the fracture behavior is more complex and hierarchical. These features further support that A-2 is more consistent with ductile fracture (35). When subjected to force, composites change from brittle fracture to ductile fracture in the presence of macromolecules with different moduli from the resin matrix. Several holes can be seen in Figure 10b. When the material is subjected to an external force, the dispersed NBR powder produces a stress concentration effect, which causes the surrounding matrix to generate three-dimensional tension. The NBR powder releases its elastic strain energy through cavitation and interface debonding to achieve the toughening effect further.

The morphology of the resin-fiber interface is shown by the SEM analysis in Figure 11. The glass fibers in Figure 11a are all covered with resin. In Figure 11b, some fibers are exposed, and there is no trace of resin on the surface of the exposed fibers. There are even obvious holes in the interface. After the addition of the rubber, the phenomenon of poor interfacial bonding becomes obvious.

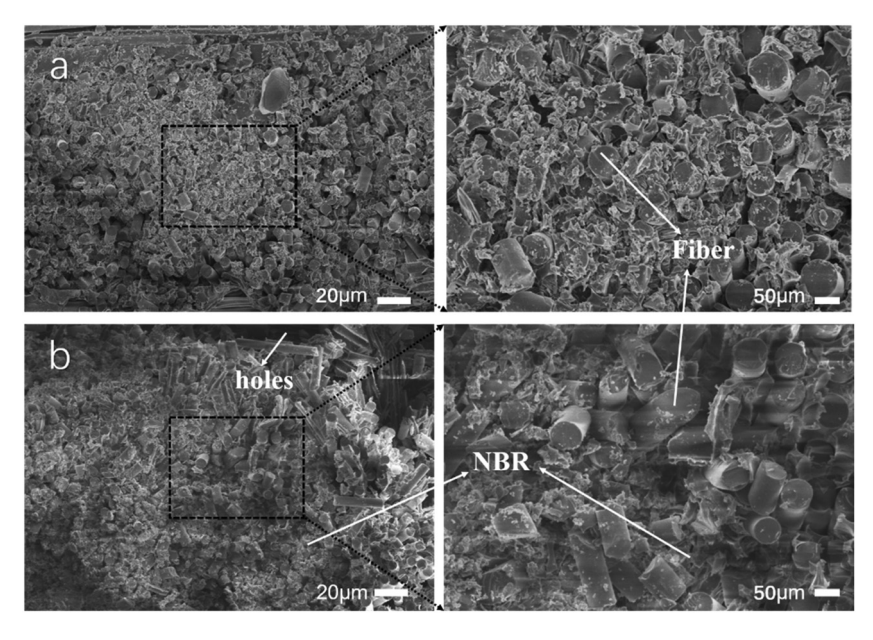


Figure 10: SEM images of fractured surfaces of composites: (a) A-0 and (b) A-2.

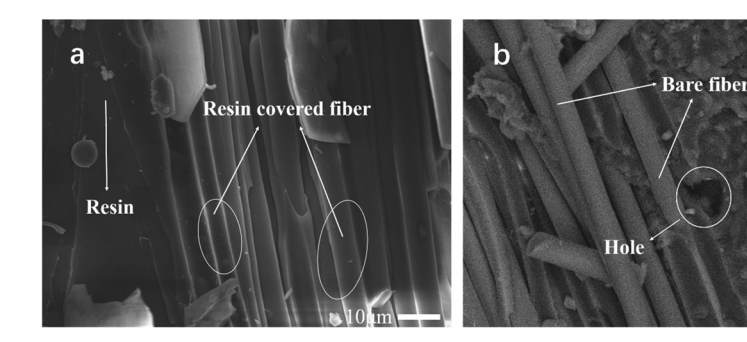


Figure 11: SEM images of interface of composites: (a) A-0 and (b) A-2.

5 Conclusion

In this article, the CTE of phenolic composites was improved by preparing rubber-modified boron-phenolic composites. The tensile strength of the NBR/BPF composites decreases from 82 to 38 MPa with the addition of powder, the elongation rate increases from 20% to 32%, and the flexural strength reaches the maximum (186 MPa) when 10 wt% NBR powder is added. Mechanical properties are well preserved at low rubber addition. The addition of NBR powder has little effect on heat resistance below 300°C, which agrees with the default usage environment. NBR powder improves the CTE. The CTE of the composites increases from $8.9 \times 10^{-6} \,\mathrm{K}^{-1}$ to $1.5 \times 10^{-5} \,\mathrm{K}^{-1}$, increasing by nearly 70%. The SEM image shows that the tensile section of the composites without NBR is characterized by brittle fracture, and the fracture is flat and without fiber pullout. The cross section of modified composites shows a tortuous fracture path. Most properties of materials are as expected, and materials can be used in aircraft parts with heavy internal stress. The controllable high CTE and interfacial issues must be addressed for stable service.

Funding information: Authors state no funding involved

Author contributions: Chenglong Zhao: writing – original draft editing, chart editing, analyzing data, process management; Yan Qin: conceptualization, resource, supervision; Xiaotian Wang: writing – original draft; Han Xiao: writing – original draft.

Conflict of interest: Authors state no conflict of interest

Data availability statements: The datasets generated during and/or analyzed during the current study are available from the corresponding author on reasonable request.

References

(1) Silva SF, Machado HA, Bittencourt E. Effect of the fiber orientation relatively to the plasma flow direction in the ablation process of a carbon-phenolic composite. J Aerosp Technol Manag. 2015;7(1):43–52. doi: 10.5028/jatm.v7i1.437.

Resin

- (2) Mirzapour MA, Haghighat HR, Eslami Z. Effect of zirconia on ablation mechanism of asbestos fiber/phenolic composites in oxyacetylene torch environment. Ceram Int. 2013;39(8):9263-72. doi: 10.1016/j.ceramint.2013.05.034.
- (3) Shaheryar A, Khan S, Qaiser H, Khurram AA, Subhani T. Mechanical and thermal properties of hybrid carbon fibre-phenolic matrix composites containing graphene nanoplatelets and graphite powder. Plast Rubber Compos. 2017;46(10):431-41. doi: 10.1080/14658011.2017.1385177.
- (4) Li ZZ, Zou ZY, Qin Y, Qi M, Ren JW, Peng ZW. The effect of fibre content on properties of ceramifiable composites. Plast Rubber Compos. 2020;49(5):230-6. doi: 10.1080/14658011.2020.1731258.
- (5) Shi X, Zhang R, Ruan K, Ma T, Guo Y, Gu J. Improvement of thermal conductivities and simulation model for glass fabrics reinforced epoxy laminated composites via introducing hetero-structured BNN-30@BNNS fillers. J Mater Sci Technol. 2021;82(23):239-49. doi: 10.1016/j.jmst.2021.01.018.
- (6) Zhang RH, Shi XT, Tang L, Liu Z, Zhang JL, Guo YQ, et al. Thermally conductive and insulating epoxy composites by synchronously incorporating Si-sol functionalized glass fibers and boron nitride fillers. Chin J Polym Sci. 2020;38(7):730–9. doi: 10.1007/s10118-020-2391-0.
- (7) Zhu XL, Tang JJ. Study on the toughening and heat resistance modification of phenolic resin. Synth Mater Aging Appl. 2019;48(6):119-22. doi: 10.16584/j.cnki.issn1671-5381.2019.06.031.
- (8) Ali HT, Akrami R, Fotouhi S, Bodaghi M, Saeedifar M, Yusuf M, et al. Fiber reinforced polymer composites in bridge industry. Structures. 2021;30:774–85. doi: 10.1016/j.istruc.2020.12.092.
- (9) Farhan S, Wang RM, Li KZ. Characterization of latticed SiC nanowires containing coating for carbon foam using carbonization activated pack cementation process. J Alloy Compd. 2016;682:695-705. doi: 10.1016/j.jallcom.2016.04.319.
- (10) Liu L, Jia C, He J, Zhao F, Fan D, Xing L, et al. Interfacial characterization, control and modification of carbon fiber

- reinforced polymer composites. Compos Sci Technol. 2015;121:56-72. doi: 10.1016/j.compscitech.2015.08.002.
- (11) Wu Q, Li W, Liu C, Xu Y, Li G, Zhang H, et al. Carbon fiber reinforced elastomeric thermal interface materials for spacecraft. Carbon. 2022;187:432–8. doi: 10.1016/j.carbon.2021.11.039.
- (12) Fotouhi S, Pashmforoush F, Bodaghi M, Fotouhi M. Autonomous damage recognition in visual inspection of laminated composite structures using deep learning. Composite Struct. 2021;268:113960. doi: 10.1016/j.compstruct.2021.113960.
- (13) Jolaiy S, Yousefi A, Mashhadi MM, Amoozgar M, Bodaghi M. Dynamic behaviors of composite leaf springs with viscoelastic cores. Mech Based Des Struc. 2021;49:1–23. doi: 10.1080/15397734.2021.1904256.
- (14) Zeinab SJ, Ehsan A, Saeed A, Mahdi B. On the higher-order thermal vibrations of FG saturated porous cylindrical microshells integrated with nanocomposite skins in viscoelastic medium. Def Technol. 2021. doi: 10.1016/j.dt.2021.07.007.
- (15) Liu NL, Qi SH, Li SS, Wu LM, Lu HL. Research progress in CTBN toughening modification of thermosetting resins. China Plast. 2011;32(3):18–24. doi: 10.19491/j.issn.1001-9278.2011.03.005.
- (16) Yan D, Li XF, Ma HL, Tang XZ, Zhang Z, Yu ZZ. Effect of compounding sequence on localization of carbon nanotubes and electrical properties of ternary nanocomposites. Compos Part A Appl S. 2013;49:35–41. doi: 10.1016/j.compositesa.2013.02.002.
- (17) Liu WW, Ma JJ, Zhan MS, Wang K. The toughening effect and mechanism of styrene-butadiene rubber nanoparticles for novolac resin. J Appl Polym Sci. 2015;132(9):41533. doi: 10.1002/app.41533.
- (18) Kazemi ME, Bodaghi M, Shanmugam L, Fotouhi M, Yang L, Zhang W, et al. Developing thermoplastic hybrid titanium composite laminates (HTCLS) at room temperature: Low-velocity impact analyses. Compos Part A Appl S. 2021;49:106552. doi: 10.1016/j.compositesa.2021.106552.
- (19) Song M, Yue X, Wang X, Huang M, Ma M, Pan W, et al. Improved high-temperature damping performance of nitrile-butadiene rubber/phenolic resin composites by introducing different hindered amine molecules. e-Polymers. 2020;20(1):482–90. doi: 10.1515/epoly-2020-0054.
- (20) Sekhar NC, Varghese LA. Rheological studies of phenolic resole resin incorporated with modified graphite additives. Chem Eng & Technol. 2021;44(50):836-43. doi: 10.1002/ceat.202000469.
- (21) Wang B, Shi MX, Ding J, Huang ZX. Polyhedral oligomeric silsesquioxane (POSS)-modified phenolic resin: Synthesis and anti-oxidation properties. 2021;21(1):316–26. doi: 10.1515/epoly-2021-0031.
- (22) Tang L, He M, Na X, Guan X, Zhang R, Zhang J, et al. Functionalized glass fibers cloth/spherical BN fillers/epoxy laminated composites with excellent thermal conductivities and electrical insulation properties. Compos Commun. 2019;16:5-10. doi: 10.1016/j.coco.2019.08.007.

- (23) Xu GM, Shuai CG. Axial and lateral stiffness of spherical self-balancing fiber reinforced rubber pipes under internal pressure. Sci Eng Composite Mater. 2021;28(1):96–106. doi: 10.1515/secm-2021-0009.
- (24) Wang HF, Liu Y, Zhang J, Yu XY, Zhang QX. Study on the properties of carboxyl-terminated liquid nitrile rubber modified phenolic epoxy resin. Thermosetting Resin. 2018;33(4):35–9. doi: 10.13650/j.cnki.rgxsz.2018.04.007.
- (25) Chen J, Zhang QZ, Hou ZS, Jin FL, Park SJ. Preparation and characterization of graphite/thermosetting composites. B Mater Sci. 2019;42(4):1–4. doi: 10.1007/s12034-019-1844-y.
- (26) Meng XY, He X, Qin Y, Zou ZY, Fu HD. Study on the quartz fiber reinforced ceramizable boron phenolic ablation resistant composite. Thermoset Resin. 2020;35(3):10-4. doi: 10.13650/j.cnki.rgxsz.2020.03.003.
- (27) Zhao J, Zhang J, Wang L, Li J, Feng T, Fan J, et al. Superior waveabsorbing performances of silicone rubber composites via introducing covalently bonded SnO₂@MWCNT absorbent with encapsulation structure. Compos Commun. 2021;22:100486. doi: 10.1016/j.coco.2020.100486.
- (28) Tang L, Zhang JL, Gu JW. Random copolymer membrane coated PBO fibers with significantly improved interfacial adhesion for PBO fibers/cyanate ester composites. Chin J Aeronaut. 2021;34(2):659–68. doi: 10.1016/j.cja.2020.03.007.
- (29) Han Y, Shi X, Yang X, Guo Y, Zhang J, Kong J, et al. Enhanced thermal conductivities of epoxy nanocomposites via incorporating in-situ fabricated hetero-structured SiC-BNNS fillers. Compos Sci Technol. 2020;187:107944. doi: 10.1016/j.compscitech.2019.107944.
- (30) Xie YW, Zheng LI, Xia Yu, Hao CG, Hao ZQ. Study on ablation and thermal insulation performance of ceramizable phenolic matrix composites. J Cap Norm Univ. 2019;40(5):52–6. doi: 10.19789/j.1004-9398.2019.05.010.
- (31) Ding J, Yang T, Huang ZX, Qin Y, Wang YB. Thermal stability and ablation resistance, and ablation mechanism of carbon-phenolic composites with different zirconium silicide particle loadings. Compos Part B-Eng. 2018;154:313-20. doi: 10.1016/j.compositesb.2018.07.057.
- (32) He YX, Sang YF, Zhang L, Yao DH, Sun KB, Zhang YQ. Coefficient of thermal expansion and mechanical properties at cryogenic temperature of core-shell rubber particle modified epoxy. Plast Rubber Compos. 2014;43(3):89–97. doi: 10.1179/1743289814Y.0000000074.
- (33) Tang HG, Ding FZ. Comparative study on properties of NBR and BNBR. Polym Bull. 2020;5:24–30. doi: 10.14028/j.cnki.1003-3726.2020.05.003.
- (34) Demir H, Dogan DM, Dogan A. Tensile properties of denture base Resin reinforced with various esthetic fibers. J Poly Sc. 2012;123(6):3354-62. doi: 10.1002/app.33831.
- (35) Li WW, Ji CY, Zhu HG, Xing F, Wu JX, Niu XL. Experimental investigation on the durability of glass fiber-reinforced polymer composites containing nanocomposite. J Nanomater. 2013;2013(1):1–11. doi: 10.1155/2013/352639.